Performance Evaluation of GPS Auto-Surveying Techniques

João Gonçalo Filipe Manito
joao.manito@tecnico.ulisboa.pt

Instituto Superior Técnico, Lisboa, Portugal

January 2021

Abstract

With the increase in widespread use of Global Navigation Satellite Systems (GNSS), more and more applications require precise position data. Of all the GNSS positioning methods, the most precise ones are those that are based in differential systems, like Differential GNSS (DGNSS) and Real-Time Kinematics (RTK). However, these systems require a very precise estimate of their reference station position to have good precision. This is the problem this thesis set out to study. Four positioning methods were analyzed, namely Least Squares (LS), Weighted Least Squares (WLS), Extended Kalman Filter (EKF) and Unscented Kalman Filter (UKF), using only pseudorange measurements. It was also tested the Hatch Filter, RAIM and statistical methods, in order to characterize several possible methods of auto-survey for a static receiver. After testing, it is seen that the EKF and UKF present much better mean error results than LS and WLS, with an attained precision below 1 meter after about 4 hours. It was also verified the importance of RAIM for the self-survey procedure. Chosen the combination of methods that gives the best results, it was tested against existing implementations showing it is very competitive, especially considering the differences between the used receivers. Finally, these results were used in a DGNSS test, which verified a significant improvement in the position estimate as the base station position estimate improves.
Keywords: GNSS, GPS, Base-station, Auto-surveying

1. Introduction

Global Navigation Satellite Systems (GNSS), of which the most famous is the Global Positioning System (GPS), are deeply woven into the fabric of our contemporaneous society.

Initially large and unwieldy, today's GNSS-enabled devices are small, sleek and inexpensive and enabled many new possibilities: self-driving vehicles, autonomous harbour freight transport, small, unmanned aircraft, etc. As a consequence, evermore accurate receivers where required, to provide more accurate position solutions for these and other new fields.

While it is possible to obtain a position estimate with a single receiver, using static reference receivers to obtain differential measurements allows much more accurate estimates. This is the basis for methods like like Differential GNSS (DGNSS) and Real-Time Kinematics (RTK).

However, this raises an important question: what is the real position of the reference receivers? This is the question that this thesis tries to answer. Using several methods, a comparative analysis of current position estimation methods will be done, with regards to both precision and time to convergence of the position solution.

2. Background

2.1. Error sources in GPS measurements

The GPS signals do not always travel in a pure vaccum and the measurement of both GPS signals and satellite positions aren't perfect. This leads to several error sources that affect the GPS signals, which can be due to the signal propagation medium (tropspheric and ionospheric errors), uncertainties in the GPS atomic clocks, ephemeris errors, multipath phenomena, relativistic effects, etc. The combination of all the previous errors result in an overall error value that is known as the User Equivalent Range Error (UERE), given by the Root-Sum-Squared (RSS) of all the different components. This error is assumed to be gaussian-distributed, and all the components are treated as independent random variables. For pseudorange measurements, the total system UERE is 7.03 meters (1σ) [1].

3. GPS Observables

The two most used GPS observables are the pseudorange and the carrier phase, which give a measure of the distance between receiver and satellite.

3.1. Pseudorange

A GPS receiver can determine its position by usage of ranging codes, using a modified version of the so called time-of-arrival (TOA) ranging method. As

such, the GPS receiver determines the distance between receiver and satellite by the time of propagation of the signal. However, since different delays and errors afect the signal the computed range won't be the true range; as such, it is given the name *pseudorange*. The distance, as seen by the receiver, between the receiver and a GPS satellite in orbit is given by

$$r = c\,(t_u - t_s) = c\Delta t \tag{1}$$

where r is the true range to the satellite, t_s is the true time of departure of the signal from the GPS satellite, t_u is the true time of arrival of the signal to the receiver, c is the speed of light in a vaccum and Δt is the true travel time of the signal.

Adding the different delays and errors, we can write a new equation for the time of arrival method using the pseudorange

$$\rho^i = r^i + c\delta t_r - c\delta t^i + T^i + I^i + MP^i + \epsilon_\rho \tag{2}$$

where δt_r and δt^i are the receiver and satellite clock errors (in seconds), T^i is the tropospheric delay (in meters) between the receiver and satellite i, I^i is the ionospheric delay (in meters) between the receiver and satellite i, MP^i is the multipath error (in meters) between the receiver and satellite i and ϵ_ρ denotes any unmodelled errors in the pseudorange.

3.2. Carrier phase

Another observable is the phase of the GPS carrier signal, with measurement resolution on the order of millimeters [2]. However, this only applies to the fractional part of the phase, since the total number of cycles since broadcast is unknown and the receiver attributes an arbitrary integer number to this component. Solving this ambiguity, a receiver can provide very accurate measurements.

In an error-free situation the carrier phase measured by a receiver r, ϕ_r, relative to satellite s is given by [2]

$$\phi_r^s = \phi_r(t) - \phi^s(t - \Delta t) + N_r^s \tag{3}$$

where $\phi_r(r)$ is the receiver-measured carrier phase at time t, $\phi^s(t - \Delta t)$ is the carrier phase at the time of transmission and N_r^s is the number of whole cycles between transmission and reception, i.e. the integer ambiguity.

Multiplying 3 by the carrier wavelength, λ, using the time of propagation to define the true range and adding the modelled error terms, we get the carrier phase model. Denoting the carrier phase in units of length, $\Phi_r^t(t)$, we can write

$$\Phi_r^s = r + c\delta t_r + c\delta t^s + \lambda N_r^s + T^i - I^i + MP^i + \epsilon_\phi \tag{4}$$

where δt_r and δt^i are the receiver and satellite clock errors (in seconds), T^i is the tropospheric delay (in meters) between the receiver and satellite i, I^i is the ionospheric delay (in meters) between the receiver and satellite i, MP^i is the multipath error (in meters) between the receiver and satellite i and ϵ_ϕ denotes any unmodelled errors in the carrier phase.

Finally, since the carrier phase depends on an arbitrary integer N, this parameter will be different every time the satellite lock is lost, a phenomenon called cycle slip and whose detection and correction is necessary. In the case of the single-frequency receiver, this detection is only indirect, while much more easier to detect in dual-frequency receivers [3].

4. Maximum Likelihood Estimation

Since GNSS position estimates are tainted by noise, we can use statistical methods to analyse their properties and give a better estimate of the true position of a GNSS antenna. One such method is the Maximum Likelihood Estimation. In this method, we use the known density probability function of the measurement data, where each sample is assumed independent, conditioned by a parameter θ and a sample set, $\mathbf{x}$. From here, we can define the likelihood function, $\mathcal{L}(\theta, \mathbf{x})$, as [4]

$$\mathcal{L}(\theta|\mathbf{x}) = f_{\mathbf{X}}(\mathbf{x}|\theta) = \prod_{i=1}^{n} f_X(x_i|\theta), \quad \text{with } \theta \in \Theta \tag{5}$$

where $f_X(\,\cdot\,|\theta)$ is the probability density function of the random variable X knowing that θ is the true value of the desired parameter, θ represents, by convention, both the unknown parameter and the estimated parameter and Θ is the parametric space of possible parameters.

The Maximum Likelihood Estimate, $\hat{\theta}$ is the the argument that maximizes the likelihood function

$$\mathcal{L}(\hat{\theta}|\mathbf{x}) = \arg\max_{\theta\in\Theta} \mathcal{L}(\theta|\mathbf{x}) \tag{6}$$

One can also use the logarithm of the likelihood function, designated log-likelihood function

$$\ln\left[\mathcal{L}(\hat{\theta}|\mathbf{x})\right] = \arg\max_{\theta\in\Theta} \ln\left[\mathcal{L}(\theta|\mathbf{x})\right] \tag{7}$$

which is analytically simpler. For a continuous parametric space, we can use the normal process of finding the maxima of a function. For a given parameter vector θ with $p > 1$ number of parameters the maximum likelihood function verifies the condition

$$\left.\frac{\partial \ln\left[\mathcal{L}(\theta_1, \ldots, \theta_p|\mathbf{x})\right]}{\partial\theta_j}\right|_{\theta=\hat{\theta}} = 0, \text{ with } j = 1, \ldots, p \tag{8}$$

Then, we check if that point is a maxima of the function [5]

$$H(\theta) = \nabla^2 \ln\left[\mathcal{L}(\theta_1, \ldots, \theta_p|\mathbf{x})\right] = h_{ij}(\theta), \quad \text{with } i, j = 1, \ldots, p \tag{9}$$

where

$$h_{ij}(\theta) = \frac{\partial^2 \ln\left[\mathcal{L}(\theta_1, \ldots, \theta_p|\mathbf{x})\right]}{\partial\theta_i \partial\theta_j} \tag{10}$$

If these conditions are verified, then $\hat{\theta}$ is the maximum likelihood estimate of the parameter vector θ. This computation was done using the mle function of Matlab's Statistics and Machine Learning Toolbox.

5. Position Determination

5.1. Least Squares

Let the satellite-receiver true range be [3]:

$$r^i = \sqrt{\left(x^i - x\right)^2 + \left(y^i - y\right)^2 + \left(z^i - z\right)^2} \tag{11}$$

where $\left(x^i, y^i, z^i\right)$ are the coordinates of satellite i and (x, y, z) is the true receiver position, both in an ECEF reference frame.

Combining the pseudorange model of Equation 2 with Equation 11 and assuming the modeled errors have been removed from the pseudorange measurement we can write [6]

$$\rho^i = \sqrt{\left(x^i - x\right)^2 + \left(y^i - y\right)^2 + \left(z^i - z\right)^2} + c\delta t_r \tag{12}$$

where on the right side we obtain the four unknown parameters: receiver coordinates (x, y, z) and receiver clock offset δt_r. Since we have four unknown parameters, we will require at least four independent measurements to be able to determine all the unknown parameters.

To solve Equation 12, which is non-linear, we can apply Taylor's series expansion to the satellite-receiver range, yielding [7]

$$r^i = r_0^i + \frac{x_0 - x^i}{r_0^i}\Delta x + \frac{y_0 - y^i}{r_0^i}\Delta y + \frac{z_0 - z^i}{r_0^i}\Delta z \tag{13}$$

where $\mathbf{x_0} = (x_0, y_0, z_0)$ is the initial position estimate, r_0^i is the satellite-receiver distance computed at $\mathbf{x_0}$ and $\Delta x = x - x_0$, $\Delta y = y - y_0$ and $\Delta z = z - z_0$

Moving the term $\mathbf{r_0^i}$ to the left side, we obtain the linearized pseudorange equation for a single satellite. Expanding the system to $n \geq 4$ satellites we rewrite it in matrix notation [7]

$$\begin{bmatrix} \rho^1 - r_0^1 \\ \vdots \\ \rho^n - r_0^n \end{bmatrix} = \begin{bmatrix} \frac{x_0 - x^1}{r_0^1} & \frac{y_0 - y^1}{r_0^1} & \frac{z_0 - z^1}{r_0^1} & 1 \\ \vdots & \vdots & \vdots & \vdots \\ \frac{x_0 - x^n}{r_0^n} & \frac{y_0 - y^n}{r_0^n} & \frac{z_0 - z^n}{r_0^n} & 1 \end{bmatrix} \begin{bmatrix} \Delta x \\ \Delta y \\ \Delta z \\ c\delta t \end{bmatrix} \tag{14}$$

or, in a more compact notation

$$\mathbf{\Delta}\rho = \mathbf{H}\mathbf{\Delta}\mathbf{x} \tag{15}$$

Finaly, the solution for this equation is given by

$$\mathbf{\Delta}\mathbf{x} = \mathbf{H}^{-1}\mathbf{\Delta}\rho \tag{16}$$

or, in the case of more than four satellites by the Least Squares solution [7]

$$\mathbf{\Delta}\hat{\mathbf{x}} = \left(\mathbf{H}^\mathsf{T}\mathbf{H}\right)^{-1}\mathbf{H}^\mathsf{T}\mathbf{\Delta}\rho \tag{17}$$

and the position estimate can be calculated by updating the initial estimate with the estimated deviations

$$\hat{\mathbf{x}} = \mathbf{x_0} + \mathbf{\Delta}\mathbf{x} \tag{18}$$

A diagram illustrating the Least Squares process is given in Figure 1.

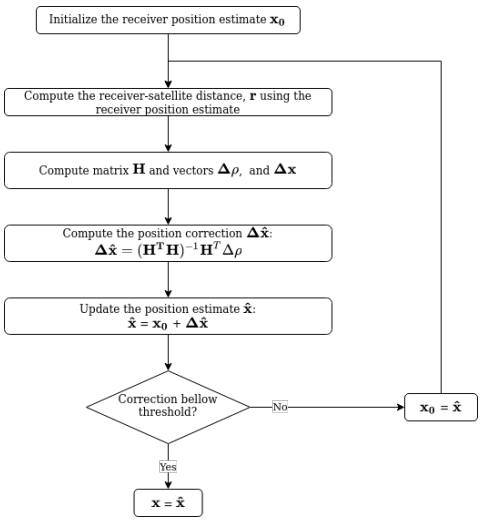

Figure 1: Least Squares algorithm

5.2. Weighted Least Squares

While the Least Squares solution assumes all errors are independent and identically distributed, this is usually not the case. By defining a weighting matrix $\mathbf{Q}$, corresponding to the inverse of the measurement error covariance matrix [8], and applying it to the Least Squares solution we obtain the Weighted Least Squares solution [8]

$$\mathbf{\Delta}\hat{\mathbf{x}} = \left(\mathbf{H}^\mathsf{T}\mathbf{Q}\mathbf{H}\right)^{-1}\mathbf{H}^\mathsf{T}\mathbf{Q}\Delta\rho \tag{19}$$

There are several possible formulations for the measurement error covariance matrix and, subsequently, for the weighting matrix [3] [8]. For the present thesis, the satellite measurements were assumed uncorrelated with standard deviation given by [9]

$$\sigma_i = \frac{\sigma_{URA_i}}{\sin\epsilon_i} \tag{20}$$

where σ_{URA_i} is the broadcasted User Range Accuracy for satellite i and ϵ_i is the satellite elevation angle. This results in a diagonal weighting matrix with elements

$$Q_i i = \frac{1}{\sigma_i^2} = \frac{\sin^2\epsilon_i}{\sigma_{URA_i}^2} \tag{21}$$

5.3. Extended Kalman Filter

A different positioning method, which takes into account the previous position estimates and the system dynamics, is the Extended Kalman Filter (EKF). The EKF works in discrete time, t_k, and for each iteration k of the filter we have two steps:

- **Prediction**, where we estimate the state vector $\hat{\mathbf{x}}_k$ using the observations from the previous iteration,
- **Filtering**, where we estimate $\hat{\mathbf{x}}_k$ using the state vector estimate of the prediction step and the current observations.

5.3.1. Dynamics model

In this thesis, the *P model* for the EKF was implemented. In this model, the state vector is [6]

$$\mathbf{x} = \begin{bmatrix} x \\ y \\ z \\ x_\phi \\ x_f \end{bmatrix} \tag{22}$$

For this case, the state transition matrix $\mathbf{\Phi}$ is given by [6]

$$\Phi = \begin{bmatrix} 1 & 0 & 0 & 0 & 0 \\ 0 & 1 & 0 & 0 & 0 \\ 0 & 0 & 1 & 0 & 0 \\ 0 & 0 & 0 & 1 & \Delta t \\ 0 & 0 & 0 & 0 & 1 \end{bmatrix} \tag{23}$$

And the noise covariance matrix is [6]:

$$Q = \begin{bmatrix} 0 & 0 & 0 & 0 & 0 \\ 0 & 0 & 0 & 0 & 0 \\ 0 & 0 & 0 & 0 & 0 \\ 0 & 0 & 0 & q_\phi & 0 \\ 0 & 0 & 0 & 0 & q_f \end{bmatrix} \tag{24}$$

where q_ϕ and q_f are associated with the Allan variance parameters. In the case of a low-cost temperature compensated crystal oscillator we get [10]

$$\begin{aligned} q_\phi &\approx \frac{h_0}{2} = \frac{2 \cdot 10^{-19}}{2} \\ q_f &\approx 2\pi^2 h_{-2} = 2\pi^2 \left(2 \cdot 10^{-20}\right) \end{aligned}$$

which, for a low-cost temperature compensated crystal oscillator are [10]

$$\begin{aligned} h_0 &= 2 \cdot 10^{-19} \\ h_{-2} &= 2 \cdot 10^{-20} \end{aligned} \tag{25}$$

From Equations 23 and 24 we can obtain the noise covariance matrix of the discrete-time dynamics dynamics model, $\mathbf{Q_k}$, as [6]

$$\mathbf{Q_k} \approx \mathbf{\Phi Q \Phi}^\mathsf{T} \Delta t \tag{26}$$

$$= \Delta t \begin{bmatrix} 0 & 0 & 0 & 0 & 0 \\ 0 & 0 & 0 & 0 & 0 \\ 0 & 0 & 0 & 0 & 0 \\ 0 & 0 & 0 & c^2\left(q_\phi + \frac{q_f \Delta t^2}{3}\right) & \frac{c^2 q_f \Delta t}{2} \\ 0 & 0 & 0 & \frac{c^2 q_f \Delta t}{2} & c^2 q_f \end{bmatrix} \tag{27}$$

where the clock variances where multiplied c^2 because the clock errors are in units of meters.

5.3.2. Observations Model

The observations equation of the EKF is given by [6]

$$\mathbf{z_k} = \mathbf{h}\left[\mathbf{x}(t_k)\right] + \mathbf{v}_k \tag{28}$$

where $\mathbf{z}_k$ is the measured pseudorange vector with $n \geq 4$ observations, $\mathbf{v}_k$ the observations noise and $\mathbf{h}\left[\mathbf{x}(t_k)\right]$ is the navigation equation vector

$$\mathbf{h}(\mathbf{x}) = \begin{bmatrix} \sqrt{\left(x^1 - x\right)^2 + \left(y^1 - y\right)^2 + \left(z^1 - z\right)^2} + c\delta t_r \\ \vdots \\ \sqrt{\left(x^n - x\right)^2 + \left(y^n - y\right)^2 + \left(z^n - z\right)^2} + c\delta t_r \end{bmatrix} \tag{29}$$

In order to linearize the navigation equations, we obtain the Jacobian matrix of 29. This matrix is called the observation matrix, $\mathbf{H}$, and is given by

$$\mathbf{H}_k = \left[\frac{\partial \mathbf{h}(\mathbf{x})}{\partial \mathbf{x}}\right]_{\mathbf{x}=\mathbf{x}_{\mathbf{k-1}}^+}, \tag{30}$$

For the P model used in this thesis, the observation matrix for n observations can be defined as

$$\mathbf{H}_k = \begin{bmatrix} a_{x_1} & a_{y_1} & a_{z_1} & 1 & 0 \\ \vdots & & & & \\ a_{x_n} & a_{y_n} & a_{z_n} & 1 & 0 \end{bmatrix} \tag{31}$$

where the elements of the observation matrix are $a_{x_i} = \frac{x^i - \hat{x}}{\hat{r}^i}$, $a_{y_i} = \frac{y^i - \hat{y}}{\hat{r}^i}$ and $a_{z_i} = \frac{z^i - \hat{z}}{\hat{r}^i}$, and the satellite-receiver range is

$$\hat{r}^i = \sqrt{\left(x^i - \hat{x}\right)^2 + \left(y^i - \hat{y}\right)^2 + \left(z^i - \hat{z}\right)^2} \tag{32}$$

Finally, the observation noise covariance matrix is given by

$$\mathbf{R}_k = \begin{bmatrix} \sigma_1^2 & & \mathbf{0} \\ & \sigma_2^2 & \\ & & \ddots \\ \mathbf{0} & & \sigma_n^2 \end{bmatrix} \tag{33}$$

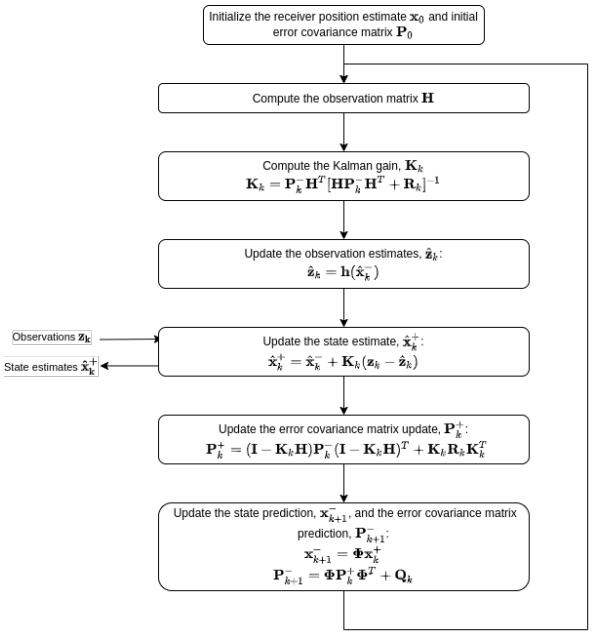

Figure 2: Flowchart of the EKF algorithm for GPS positioning [6] [11]

5.4. Unscented Kalman Filter

Another possible implementation of the Kalman Filter for a non-linear system is the Unscented Kalman Filter (UKF). In this method, instead of linearizing the non-linear model, the Unscented Transform (UF) is used to obtain the statistics of the result of the non-linear function given a set of sample points. The points used in the UT are called sigma points, and together form the sigma vector, $\mathcal{X}$. For a given iteration k, these points are given by [12]

$$\begin{aligned} \mathcal{X}_{0,k} &= \hat{x}_k \\ \mathcal{X}_{i,k} &= \hat{x}_k + \sqrt{n+\tau}\left(\sqrt{\mathbf{P}_k}\right)_i \quad \text{with } i = 1,\ldots,n \\ \mathcal{X}_{i+n,k} &= \hat{x}_k - \sqrt{n+\tau}\left(\sqrt{\mathbf{P}_k}\right)_i \end{aligned} \tag{34}$$

where n is the size of $\mathbf{x}$, τ is the scale factor of the sampling and $\left(\sqrt{P_k}\right)_i$ designates the i-th line of $\sqrt{P_k}$ and $\sqrt{P_k}$ can be obtained using the Cholesky decomposition [12]. After this sampling, the sigma points are propagated through the non-linear function $\mathbf{f}$

$$\mathcal{Y}_i, k = \mathbf{f}\left(\mathcal{X}_{i,k}\right) \qquad \text{with } i = 0,\ldots,2n \tag{35}$$

and then the statistics of the resulting vector can be obtained by means of a weighted average [12], from which we can determine the mean and covariance matrix

$$\begin{aligned} \hat{\mathbf{y}_k} &= \sum_{i=0}^{2n} W_i \mathcal{X}_{i,k} \\ \mathbf{P}_{yy} &= \sum_{i=0}^{2n} W_i \left(\mathcal{Y}_{i,k} - \hat{\mathbf{y}_k}\right)\left(\mathcal{Y}_{i,k} - \hat{\mathbf{y}_k}\right)^{\mathsf{T}} \end{aligned} \tag{36}$$

where the weight values W_i are given by

$$\begin{aligned} W_0 &= \frac{\tau}{n+\tau} \\ W_i &= \frac{1}{2\left(n+\tau\right)} \end{aligned} \tag{37}$$

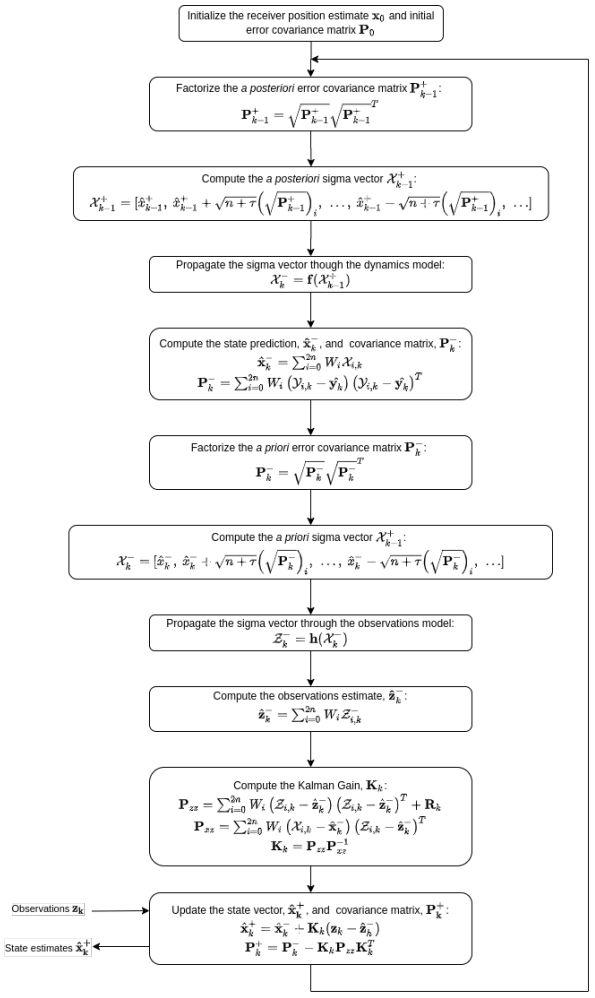

Figure 3: Flowchart of the UKF algorithm for GPS positioning [12]

5.5. Carrier-Smoothed Code - the Hatch Filter

A set of techniques that allow the incorporation of the very precise carrier phase measurements in the position estimation wihout explicitly solving the integer ambiguity problem are the Carrier-Smoothed Code (CSC) methods. One such method is the

Hatch Filter. The weighting factors $W(n)$ for the Hatch Filter, which are used to weight the influences of the carrier phase and pseudorange measurements in the smoothed result are given by

$$W(n) = W(n-1) - \gamma \tag{38}$$

The weighting factor must be initialized in its first iteration, for which we use the case where only the pseudorange measurement is used:

$$W(1) = 1 \tag{39}$$

Finally, the Hatch Filter equation is

$$\rho_{s,k} = W(n)\rho_k + (1 - W(n))\left(\rho_{s,k-1} + \Phi_k - \Phi_{k-1}\right) \tag{40}$$

where γ is the averaging constant and defines the averaging interval for the filter. Usually, it is set as 0.01 or 0.02, for a smoothing interval respectively of 100 or 50 seconds at 1Hz [13]. However, this filter is corrupted by cycle slips and must be reinitialized whenever they occur.

5.6. Differential GPS

Since this thesis' theme is the positioning of base stations for DGNSS techniques, it makes sense to use one of those techniques to validate the obtained results. The method used in this thesis is the Double-Difference pseudorange method, also called Code-Equivalent GPS Interferometer. The configuration of this system for two receivers and two satellites is given in Figure 4 , where m and k are,

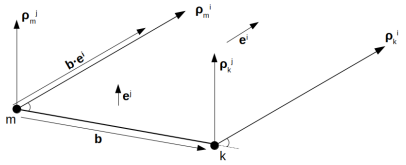

Figure 4: GPS interferometer configuration for twp satellites

respectively, the reference and rover receivers, ρ_j^i is the pseudorange between receiver j and satellite i, $\mathbf{e}^i$ is the direction vector to satellite i, $\mathbf{b}$ is the vector from the reference to rover receivers, called baseline vector and $\mathbf{b}\cdot\mathbf{e}^i$ is the projection of $\mathbf{b}$ along the direction of $\mathbf{e}^i$

Let us also consider that the distance between the receivers and satellite is much greater than the distance between receivers, which results in considering the GPS signal a planar wave at the receivers and that both receivers share the same direction vectors. Also, assume that the receivers are at approximately the same height, ensuring a similar tropospheric error. By using the pseudorange model of Equation 2 for both receivers, we can differentiate the measurements from the same satellite between the receivers, cancelling out the tropospheric, ionospheric, multipath and satellite clock bias terms. This difference is called Single Difference (SD) and is given by

$$SD_{km}^i = \rho_k^i - \rho_m^i = r_{km}^i + c\delta t_{km} + \epsilon_{\rho,km}^i \tag{41}$$

where the subscript km represents the difference between receiver k and m for each parameter and m was chosen as the reference receiver. From Figure 4 it is clear that the SD also corresponds to

$$SD_{km}^i = \mathbf{b}\cdot\mathbf{e}^i \tag{42}$$

Adding a second satellite, a new SD can be obtained. By differencing these two SD, the receiver clock bias term is cancelled out. This new difference is the Double Difference and is given by

$$DD_{km}^{ij} = SD_{km}^i - SD_{km}^j = r_{km}^{ij} + \epsilon_{\rho,km}^{ij} \tag{43}$$

where the superscript ij denotes between which satellites the difference is taken. We can also apply the DD to Equation 42 to obtain the relationship between the DD and the baseline vector:

$$DD_{km}^{ij} = \mathbf{b}\cdot\mathbf{e}^i - \mathbf{b}\cdot\mathbf{e}^j = \mathbf{b}(\mathbf{e}^i - \mathbf{e}^j) = \mathbf{b}\cdot\mathbf{e}^{ij} \tag{44}$$

For this interferometer, the DD are all taken in relation to the same satellite, which is the one with highest elevation. Combining Equations 43 and 44 for n satellites we obtain the system

$$\begin{bmatrix} DD_{km}^{12} \\ DD_{km}^{13} \\ \vdots \\ DD_{km}^{1n} \end{bmatrix} = \begin{bmatrix} e_x^{12} & e_y^{12} & e_z^{12} \\ e_x^{13} & e_y^{13} & e_z^{13} \\ \vdots & \vdots & \vdots \\ e_x^{1n} & e_y^{1n} & e_z^{1n} \end{bmatrix} \begin{bmatrix} b_x \\ b_y \\ b_z \end{bmatrix} + \begin{bmatrix} \epsilon_{km}^{12} \\ \epsilon_{km}^{13} \\ \vdots \\ \epsilon_{km}^{1n} \end{bmatrix} \tag{45}$$

which can be written in a more compact notation as

$$\mathbf{y} = \mathbf{B}\cdot\mathbf{b} + \mathbf{e} \tag{46}$$

where $\mathbf{y}$ is the measured pseudorange DD vector, $\mathbf{B}$ is the matrix of the components of the differenced direction vectors, $\mathbf{b}$ is the baseline vector and $\mathbf{e}$ is the measurement noise vector.

The baseline vector can then be determined using for example a Least Squares method or a Kalman Filter. In this case, we implemented a very simple Kalman Filter with $\mathbf{x} = \mathbf{b}$, $\mathbf{\Phi} = \mathbf{I}_3$, $\mathbf{Q} = \mathbf{0}_{3\times3}$ and $\mathbf{H} = \mathbf{B}$

5.7. RAIM

The Receiver Autonomous Integrity Monitoring (RAIM) techniques allow a GPS receiver to detect faulty satellites measurements that will degrade the position solution [3].

Most of the RAIM algorithms follow the following generic sequence of steps given a navigation solution [14]:

1. Use a detection parameter, the test statistic, to detect the presence of a fault
2. Use the expected system noises and test statistic relationship to describe a faulty measurement
3. Establish a detection threshold based on the desired probability of false alarm
4. Obtain the test statistic for each observation and perform the fault detection
5. If there are detected faults, apply some method to isolate the faulty satellite
6. Compute the protection levels (optional)

In this thesis, the focus will be on conventional RAIM techniques, with Fault Detection (FD) and Fault Detection and Exclusion (FDE) algorithms based on Least Squares Residuals (LSR).

5.7.1. Fault Detection

This algorithm is responsible for checking for anomalies in the received measurements and requires at least 5 satellites. It works by dividing the visible constellation into several subsets and using that information to find the faulty satellite. For 5 satellites, since no redundancy exists, this algorithm is merely informative.

5.7.2. Fault Detection and Exclusion

This algorithm, applicable only to sets of more than 5 satellites, excludes one satellite from each subset and repeats the FD algorithm until it finds a subset that won't degrade the position solution.

5.8. Least Squares Residuals

For a set of pseudorange measurements, and using the Least Squares solution, $\mathbf{\Delta\hat{x}}$, given by Equation 17, we can obtain an estimate of the prefit-residuals vector

$$\mathbf{\Delta}\hat{\rho} = \mathbf{H}\mathbf{\Delta}\hat{\mathbf{x}} \tag{47}$$

From here, we can calculate the range residuals, $\mathbf{w}$ [15]:

$$\mathbf{w} = \mathbf{\Delta}\rho - \mathbf{\Delta}\hat{\rho} = \mathbf{\Delta}\rho - \left(\mathbf{H}^{\mathsf{T}}\mathbf{H}\right)^{-1}\mathbf{H}^{\mathsf{T}}\mathbf{\Delta}\rho \tag{48}$$

For fault detection, we use the sum of squared errors, SSE, as an error metric

$$SSE = \mathbf{w}^{\mathsf{T}}\mathbf{w} \tag{49}$$

And then compute the test statistic, given by [15]

$$t = \sqrt{\frac{SSE}{n-4}} \tag{50}$$

where n is the number of satellites used in the FD algorithm. From here, a threshold λ can be defined to perform a binary decision where $t \geq \lambda$ is considered a fault and $t < \lambda$ is not. The detection threshold is dependent on the false alarm probability, P_{fa}, and the number of visible satellites, n, and cab be calculated by inverting the incomplete gamma function [16]

$$1 - P_{fa} = \frac{1}{2^a\Gamma(a)}\int_0^{\lambda^2} e^{-\frac{s}{2}}s^{a-1}ds \tag{51}$$

where $a = (n-4)/2$ and the gamma function is given by

$$\Gamma(x) = \int_0^{\infty} e^{-t}t^{x-1}dt\,, \text{with } x \in \mathbb{R}^+ \tag{52}$$

6. Experimental Results

In this chapter, the experimental methods and results are summarily described.

6.1. Experimental Setup

Data collection for this thesis was done using two different types of receivers, two u-blox 6T receivers and an Ashtech ProFlex 500 receiver, as well as different antennas and some processing software. All the receivers were connected to a laptop computer which provided both serial communication handling and Internet Protocol (IP) communication. All the used antennas were located at the top of the North Tower of Instituto Superior Técnico.

6.2. Antenna reference position determination

In order to validate the experimental results, it was necessary to compute an accurate estimate of the antennas' true position. This was done by processing the data collected over a long survey window with Precise Point Position algorithms. In this thesis, this was done by using IGS products and the RTKLIB software, using a methodology similar to the one described in [17]. The calculated positions for each receiver are presented in Table 1

Ant	X (m)	Y (m)	Z (m)
RF3	4918525.5233	-791212.0300	3969762.2262
RF6	4918532.1188	-791212.5264	3969754.7230
RF4	4918524.4824	-791213.3897	3969763.1602

Table 1: PPP position results for the used antennas

6.3. Algorithm validation using IGS station data

6.3.1. Positioning algorithm validation

In order to validate the developed algorithms, they were run against 24 hours of GNSS data from ESA's Malargüe Satellite Tracking Station in Mendoza, Argentina. An initial implementation saw a very large initial error with both EKF and UKF due to mismatches between the initial position error estimate and the actual error. This was solved by initializing the EKF and UKF with a LS result, which greatly decreased the initial error and convergence

time. After this change the obtained results are presented in Figure 5 and Table 2.

Error Metric	LS	WLS	EKF	UKF
Mean (m)	1.330	1.064	0.986	0.986
DRMS (m)	2.155	1.885	0.644	0.644
MRSE (m)	3.438	3.087	0.915	0.915

Table 2: Error metrics for the reference receiver after correction of initial position

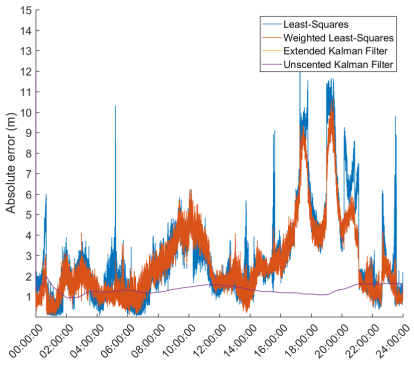

Figure 5: Absolute position error for the reference receiver after correction of initial position

6.3.2. Hatch filter validation

After validating the positioning methods, the Hatch Filter performance for different filtering parameters was tested, in order to choose the best one to apply to the rest of the experimental results. Also, since the Hatch Filter is dependent on cycle slip detection, a simple algorithm based in the difference between the smoothed and unsmoothed pseudoranges was implemented. For filtering constants of 0.005, 0.01, 0.015 and 0.02, it was observed that a higher constant improves the error of the LS and WLS, while slightly increasing the spread of the solutions, while for the EKF and UKF a lower constant yielded better results. A middle-ground value of $\gamma = 0.010$ was then chosen for the rest of the simulations.

6.4. Reference Station antenna position determination

Applying the methods to the survey data of antenna RF3, which will work as a reference station, the obtained results are presented in Table 3.

From these results, it is clear that both EKF and UKF present a much more precise and accurate position solution, with an error bellow meter-level. The Hatch Filter also results in a lower spread for the LS and WLS results, but produces a slightly higher mean error, while for the EKF and UKF the effect is oposite.

6.5. Convergence over time of the position solution

Another important metric is the time necessary for the position solution to converge to below a given error threshold, since not all base stations are permanent and only a short survey might be possible. As such, the mean error over time was computed and is presented in Figures 6 and 7.

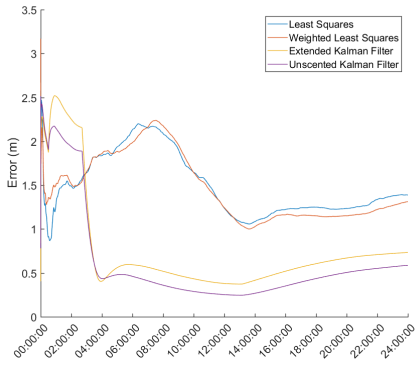

Figure 6: Mean error variation over time for the reference station antenna with no Hatch Filter

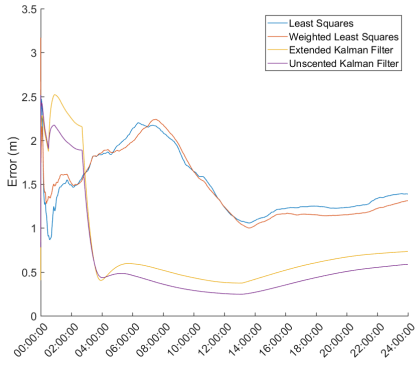

Figure 7: Mean error variation over time for the reference station antenna with Hatch Filter and $\gamma = 0.010$

From these results, we see that the Hatch Filter doesn't change the overall mean error dynamic and that even though both the Extended and Unscented Kalman Filters present a higher initial error, their mean error falls bellow the mean error of the Least Squares methods relatively quickly, in just a few hours. Even accounting for sharp decreases due to constellation changes, the EKF and UKF show a clear trend of more precise results with lesser variation after a few hours, with the UKF having the lead in precision. The error increase after approximately 13 hours of surveying is most likely due to constellation changes, as can be seen from Figure 8, where there is a jump in the GDOP parameter to much higher values.

	No Hatch Filter				Hatch Filter with $\gamma = 0.01$			
Error Metric	**LS**	**WLS**	**EKF**	**UKF**	**LS**	**WLS**	**EKF**	**UKF**
Mean (m)	1.386	1.300	0.750	0.602	1.388	1.312	0.732	0.587
DRMS (m)	1.589	1.557	0.818	0.750	1.341	1.377	0.826	0.755
MRSE (m)	2.264	2.249	1.558	1.349	1.990	2.028	1.565	1.355

Table 3: Error metrics for 24 hour position survey of the Reference Station Antenna

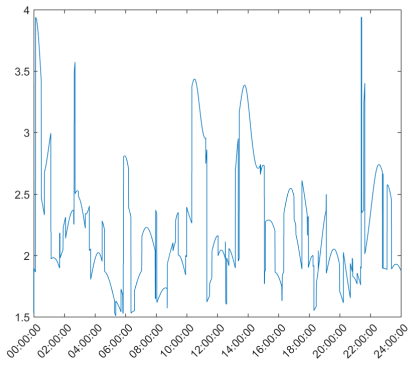

Figure 8: GDOP values for the 24 hour survey of the reference station antenna

6.6. Improving the position estimate with statistical methods

Another possibility to improve the position estimate of the receiver is using statistical methods to obtain a better "average" value. To this end, a few methods were implemented.

6.6.1. The median as position estimate

This measure, given by the point that separates a data set in two halfs, is designed to avoid biases from fringe results. Applying this method to the survey of the reference station, an increase in position estimate error, with and without the Hatch Filter. As such, this leads us to exclude this method as viable.

6.6.2. The weighted average as position estimate

Another possible method to determine the position estimate is the weighted average. By attributing weights according to a specific criterion, an average that disregards worse solutions is achieved. In this case, the weighting was done using the inverse of the GDOP parameter, de-weighting solutions with lower expected accuracy. The results obtained from this method show a slight increase in the position error, which makes this method, using the GDOP weighting criterion, unsuitable for position estimation.

6.6.3. The MLE as position estimate

This method is based in the Maximum Likelihood Estimation of Section 4. While initially both Normal and t-Location Scale distributions were considered for analysis, the MLE for the t-Location Scale was unable to converge and only results pertaining to the Normal distribution were used in this analysis. The results of the MLE with Normal distribution are exactly the same as the previously determined mean, which is expected since the ML estimator of the Normal distribution is the mean, resulting in no improvement.

6.7. Filtering using a threshold

Instead of using all the data points, it is possible to condition the data by imposing some filtering condition with an associated threshold. For position data, this can be accomplished by filtering the solutions above a multiple of the standard deviation, σ. Two different threshold were used: 1σ and 2σ. For the 2σ threshold, the EKF and UKF present a lower errror, but allow greater variation in the data; meanwhile, for the LS and WLS, this greater variation allows an increase in the estimate error. For the 1σ threshold, the results show significantly smaller variations but an increase in the mean error.

6.8. Final proposed positioning method

In order to more accurately compare each method for their merits, the combination that gives the best overall performance for each method was chosen. For the LS and WLS this corresponds to a Hatch Filter with $\gamma = 0.010$, estimate given by the measurements' mean and no thresholding, and for the EKF and UKF the same methods but with a 2σ threshold. The error measurements in these conditions are presented in Table 4.

Error Metric	**LS**	**WLS**	**EKF**	**UKF**
Mean (m)	1.386	1.300	0.694	0.584
DRMS (m)	1.589	1.557	0.740	0.676
MRSE (m)	2.264	2.249	1.370	1.177

Table 4: Error metrics for 24 hour position survey of the reference station antenna using the finalized position methods

These results confirm that EKF and UKF show much better results than LS and WLS in all metrics, and as such they will be the selected methods for base station position estimation.

6.9. Impact of RAIM in auto-surveying

In order to test how this algorithm impacts the position estimate, and in the absence of real RAIM events, several different failures were added to the

survey from Section 6.4. These consist in a 15 meter pseudorange bias between epoch 100 and 200, a 30 meter pseudorange bias between epoch 3000 and 3500 and a ramp bias, growing at the rate of 1 meter per second, between epochs 10000 and 12000, applied to random satellites in the sub-constellation that was used at that epoch. The RAIM algorithm was run with a probability of false alarm of 8×10^{-7} [18]. The position error results with and without RAIM are presented in Figures 9 and 10. The error metrics for the entire observation are also presented in Table 5. These results were obtained without the Hatch Filter.

Error Metric	LS	WLS	EKF	UKF
Mean (m)	1.391	1.300	0.801	0.649
DRMS (m)	1.592	1.575	0.806	0.739
MRSE (m)	2.272	2.276	1.574	1.361

Table 5: Error metrics for 24 hour position survey of the Reference Station Antenna after RAIM test

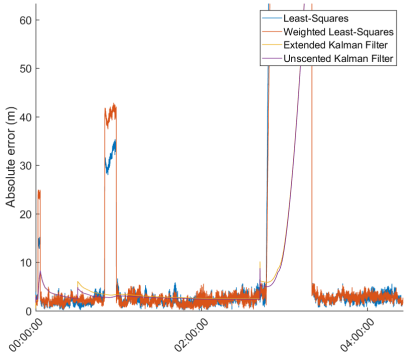

Figure 9: Reference station receiver error in the presence of simulated faulty satellites without RAIM

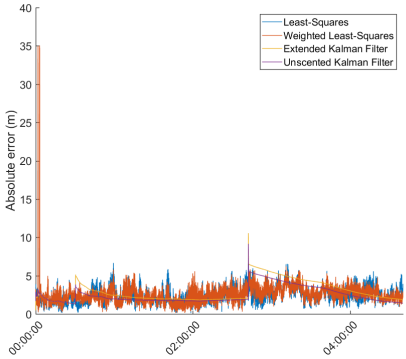

Figure 10: Reference station receiver error in the presence of simulated faulty satellites with RAIM FDE algorithm

From these results, it is clear that the RAIM algorithm can prevent big position errors in the present of faults, although only higher than a certain threshold due to the chosen probability of false alarm. This shows the validity of RAIM augmentation even in the case of a static receiver.

6.10. Performance comparison with existing auto-survey methods

In order to benchmark our methods, we must compare them with a known auto-survey method, using the Survey-In mode for the u-blox 6T receivers and RTKLIB in static mode for the ProFlex 500 receiver. These surveys were done in the same conditions and for the same time, and the results are presented in Figure 11. Comparing these results with the results presented in Figures 6 and 7, we see that the EKF and UKF methods proposed provide a signifficantly better estimate than the Survey-In mode, and, although worse, are moderately close to those obtained by the ProFlex 500 receiver, within approximately 25 centimeters of each other, which is much higher quality than the receiver used in the survey.

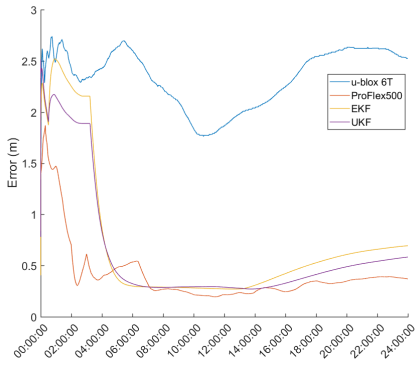

Figure 11: Auto-survey results for the u-blox 6T and ProFlex receivers for a 24 hour survey

6.11. Differential GPS test

As a final performance test, the previous methods were applied to a Double Difference DGPS setup in order to determine the position of a rover receiver. This made use of two u-blox 6T receivers, one connected to antenna RF2 and another to RF6, and the antenna position estimate was taken at 4 hour intervals with both EKF and UKF. The results are presented in Figures 12 and 12 and the mean error is presented in Table 6, and clearly show that both EKF and UKF produce accurate position estimates for the base station, resulting in a sub-meter error for the rover position.

7. Conclusions

With this work, it was shown that the EKF and UKF provide much better position estimates than the LS and WLS methods. It was also seen that the

	Extended Kalman Filter						Unscented Kalman Filter					
Hours	4	8	12	16	20	24	4	8	12	16	20	24
Mean error (m)	0.732	0.794	0.661	0.787	0.903	0.932	0.767	0.677	0.506	0.584	0.686	0.719

Table 6: Mean error for the DGPS receiver with base station position averaged after a set number of hours

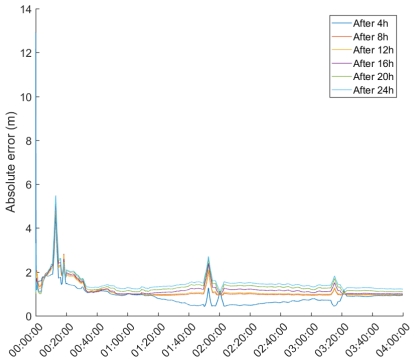

Figure 12: Rover position error with base station position obtained with EKF and averaged after a set number of hours

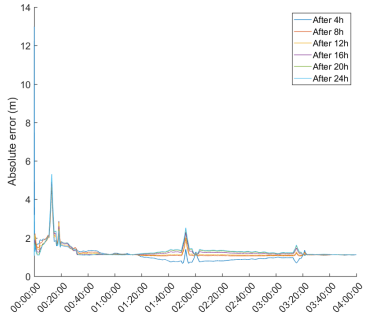

Figure 13: Rover position error with base station position obtained with UKF and averaged after a set number of hours

Hatch Filter shows mild improvements to the LS and WLS methods, but only small improvements for EKF and UKF, and that a 2σ threshold for the position estimates bennefits the EKF and UKF, with slight improvements to the WLS and a degradation to the LS methods. These results prompted the sole use of EKF and UKF as position estimation methods. Finally, a DGPS setup was used to simulate a DGPS positioning scenario, validating the previous results and achieving sub-meter accuracy for the rover position estimate.

Acknowledgements

The author would like to thank his supervisor and tutor, Prof. José Sanguino, for all his support during his time at IST and especially during this thesis. He would also like to thank Instituto de Telecomunicações (IT) for all the resources that were made available, which possibilitated this work.

References

[1] Mohinder S. Grewal. *Global Positioning Systems, Inertial Navigation, and Integration*. Wiley, John & Sons, Incorporated, 2001.

[2] Yan Xu (auth.) Guochang Xu. *GPS: Theory, Algorithms and Applications*. Springer-Verlag Berlin Heidelberg, 3 edition, 2016.

[3] Elliott D Hegarty, Christopher; Kaplan. *Understanding GPS/GNSS*. Artech House, 3rd ed edition, 2017.

[4] Thiagalingam Kirubarajan Yaakov Bar-Shalom, X. Rong Li. *Estimation with applications to tracking navigation*. Wiley-Interscience, 1 edition, 2001.

[5] Manuel Cabral Morais. *Notas de apoio da disciplina de Probabilidades e Estatística*. Instituto Superior Técnico, 2010.

[6] Fernando Duarte Nunes. *Sistemas de Controlo de Tráfego - Apontamentos das Aulas*. Instituto Superior Técnico, 2017.

[7] José E. Sanguino. *Sistemas de Navegação - Apontamentos das Aulas*. Instituto Superior Técnico, 2017/2018.

[8] K. Borre Gilbert Strang. *Linear algebra, geodesy, and GPS*. Wellesley college, 1997.

[9] Anh Quan Le. Achieving decimetre accuracy with single frequency standalone gps positioning. In *Proceedings of the 17th International Technical Meeting of the Satellite Division of The Institute of Navigation (ION GNSS 2004)*, pages 213–237, 2004.

[10] Robert Grover Brown and Patrick Y. C. Hwang. *Introduction to Random Signals and Applied Kalman Filtering with Matlab Exercises*. Wiley, 4 edition, 2012.

[11] Mark Wickert and Chiranth Siddappa. Exploring the extended kalman filter for gps positioning using simulated user and satellite track data. In *Proceedings of the 17th Python in Science Conference (SCYPI 2018)*, pages 84–90, 01 2018.

[12] Fule Zhu, Yanmei Zhang, Xuan Su, Huan Li, and Haichao Guo. GNSS position estimation based on unscented Kalman filter. *2015 International Conference on Optoelectronics and Microelectronics (ICOM)*, pages 152–155, 07 2015.

[13] K. Mazher, M. Tahir, and K. Ali. GNSS pseudorange smoothing: Linear vs non-linear filtering paradigm. In *2016 IEEE Aerospace Conference*, pages 1–10, 2016.

[14] João Pedro Duque Duarte. Integrity monitoring techniques in GPS/Galileo. Master's thesis, Instituto Superior Técnico, 2015.

[15] Fernando Duarte Nunes. *Notes on RAIM*. Instituto de Telecomunicações - Instituto Superior Técnico, 2011.

[16] Bocheng Zhu Junren Sun, Zun Niu. Fault detection and exclusion method for a deeply integrated bds/ins system. *Sensors*, 20, 03 2020.

[17] Gino Dardanelli, Claudia Pipitone, Antonio Angrisano, Salvatore Gaglione, and Anna Innac. Performance Assessment of PPP Surveys with Open Source Software Using the GNSS GPS–GLONASS–Galileo Constellations. *Applied Sciences (Switzerland)*, 10, 2020.

[18] ICAO. *AN-WP/7556 Addendum No.1 Appendix, Draft amendment to Annex 10 of the Convention on International Civil Aviation, Volume I - Radio Navigation Aids*.